Research Article

Jabulani Matsimbe*

Comparative application of photogrammetry, handmapping and android smartphone for geotechnical mapping and slope stability analysis

https://doi.org/10.1515/geo-2020-0213
received August 20, 2020; accepted November 10, 2020

Abstract: With increasing awareness of geotechnical risks in civil and mining structures, taking advantage of smartphone technology to study rocky slopes can play a key role in the development of safe and economical structures for human welfare. In Malawi, there is a research gap on application of portable devices to collect geotechnical data. Geological engineers still use the unsafe tedious handmapping technique to collect geotechnical data. A road cut that experiences frequent rockfall is used as a case study to investigate if there is a role for smartphones in geotechnics by comparing set statistics of data clusters collected through photogrammetry, smartphone and clar inclinometer. Besides low cost, smartphone' data capture speed is faster than clar inclinometer. Stereographic and kinematic analysis shows that the 75° dipping road cut is predominantly prone to wedge failure with minor planar failure. For slope stability, *Q*-slope suggests a new slope angle of 60–66°. An acceptable tolerance limit or error between handmapping and remote data capture systems should be less than ±15°. Set analysis on 111 comparable data points gave a maximum pole vector difference of 10.5°, with the minimum having a difference of 4.8°. For dip, the standard deviations vary from 4.9 to 9.5°, while their mean values vary from –2 to 2.75°. For dip directions, the standard deviations vary from 3.2 to 4.3°, while their mean values vary from –6 to 0.75°. Therefore, android smartphones have a role in geotechnics due to their allowable orientation errors, which show less variance in measured dip/dip direction.

Keywords: discontinuities, excavation, geology, Malawi, reliability

1 Introduction

A good understanding of rockmass structure forms the basis of rock mass classification, which is used in the majority of geomechanics [1]. Structural and mechanical analyses of rock masses using different mapping methods provide input data required for end-use applications such as design of surface excavations or slope stability assessments [2]. A rock mass is described as an intact rock separated by discontinuities. According to ref. [3], slope stability in surface excavations is principally a function of the structural discontinuities within the rock mass, and not the strength of the intact rock, requiring a detailed knowledge of the effect of discontinuities on the rock mass. Modern measuring technologies give the means to perform tasks previously impossible with conventional methods. Their main advantages include reduced time consumption and higher measurement precision [4]. With three-dimensional (3D) laser scan surveys, a dense point cloud is generated that represents the geometry of the scanned rock face in very high detail [5]. Nowadays, the advent of new technologies has led to step-change increase in the quality of data available for the study of rock slopes, and these include new remote sensing sensors, platforms, new techniques and software for engineering rock mass analyses [6,7]. With the advancements in artificial intelligence methods and utilization of Citizen Science (CitSci), the collection and classification of geodata from big datasets have become relatively easier thereby filling the gaps in the landslide hazard assessment process [8,9]. In Malawi, smartphone technology is rarely used in geotechnical mapping despite facing a lot of slope failures in surface excavations, which affect the safety of the people and their economic well-being as the roads become inaccessible. For example, slope failures and rock falls along the Blantyre–Chikwawa road provide a challenge for road users to conduct their businesses. Little or no knowledge exists on the usage of portable devices such as smartphones for geotechnical mapping in Malawi. Most research has been toward understanding the geology and mineralization of rocks

* **Corresponding author: Jabulani Matsimbe,** Department of Mining Engineering, Faculty of Engineering, The Polytechnic, University of Malawi, Blantyre, Malawi, e-mail: jmatsimbe@poly.ac.mw

Open Access. © 2021 Jabulani Matsimbe, published by De Gruyter. This work is licensed under the Creative Commons Attribution 4.0 International License.

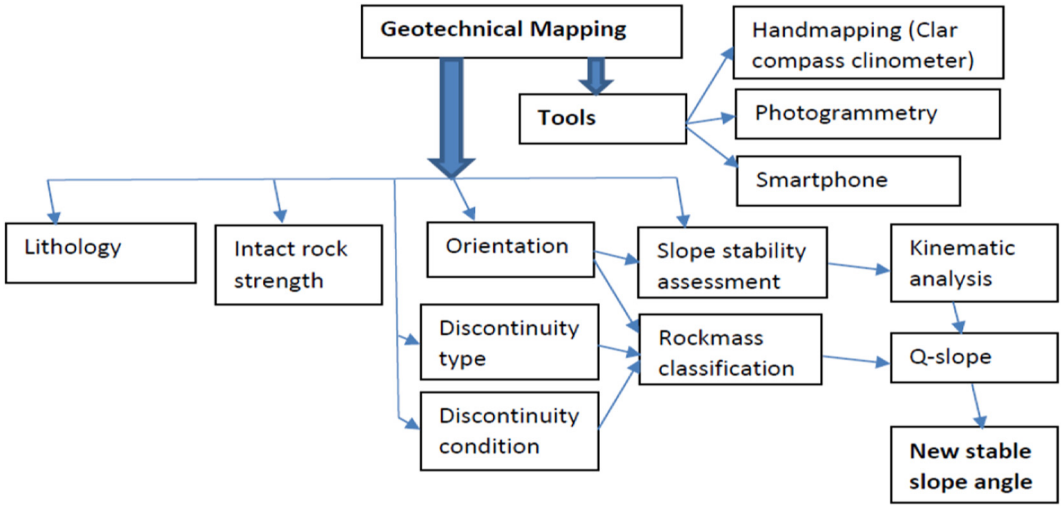

Figure 1: Geotechnical mapping flow chart with different mapping tools.

in Malawi [10]. Thus, in order to assess the possibility of using smartphones as a reliable tool for rockmass classification and slope stability analysis, this research comparatively applied photogrammetry, handmapping and android smartphone to gather input data for end-use purposes. Figure 1 gives an illustration of the geotechnical properties observed on site and the tools for collecting the geotechnical data. It is expected that the results from present study will promote the use of simple to use portable smartphones in geotechnical engineering. These gadgets are readily available and affordable to a lot of people or companies. In addition, the University curricula will be revised to incorporate smartphone technology in engineering projects.

Therefore, this article presents the findings on the comparative application of hand mapping, digital terrestrial photogrammetry and smartphone at a road cut, to remotely acquire discontinuity orientation data and their subsequent use in Photoscan to create a three-dimensional (3D) image, which is imported into SplitFX and Dips for kinematic analysis. In addition, the collected data are used to quantify the rockmass based on the rock mass rating (RMR), geological strength index (GSI), *Q*-system and *Q*-slope value. Close-range terrestrial digital photogrammetry is commonly used to capture faces of objects not more than 300 m away from the camera [11,12]. In addition, refs [13,14,2,15] have highlighted the accuracy and potential of photogrammetric techniques.

RMR is a geomechanical classification system for rocks, which gives an index value based on uniaxial compressive strength of rock, rock quality designation (RQD), spacing of discontinuities, condition of discontinuities, groundwater conditions and orientation of discontinuities [16]. The GSI is used for the estimation of the rock mass strength and the rock mass deformation modulus based on the rock structure and block surface conditions [17]. *Q*-slope is an empirical rock slope engineering method for assessing the stability of excavated rock slopes and is intended for use in reinforcement-free site access road cuts, roads or railway cuttings or individual benches in open cast mines [18]. *Q*-slope utilizes similar parameters to the *Q*-system, which has been used for over 40 years in the design of ground support for tunnels and underground excavations in the field.

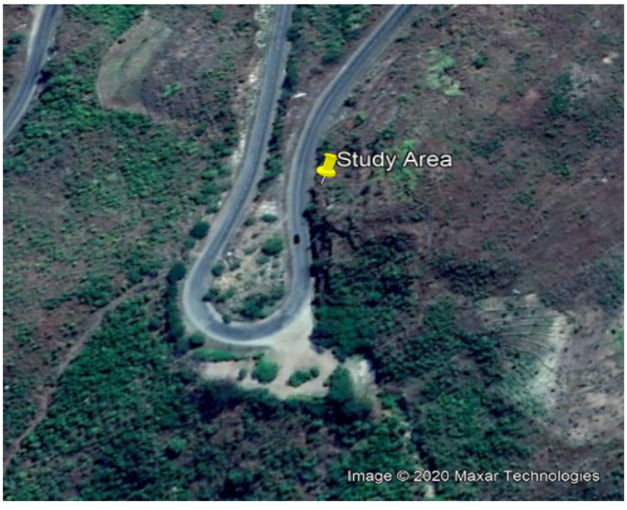

Figure 2: Location of the study area along Blantyre–Chikwawa road near Kamuzu view.

2 Methodology

Figures 2 and 3 show the location of the study area along the Blantyre–Chikwawa road at Latitude –15.953781° and Longitude 34.922827°. The granitic rock face has a blocky structure with well-defined joint sets. The geology of Malawi is part of Kibaran orogeny formed through continental collision that constructed Rodinia as known in Africa [27]. Malawi is primarily composed of Archean and Paleoproterozoic (Ubendian) terrain, which is dominated by the Basement Complex rocks later overlain by Karoo sedentary rocks and intruded by basaltic/dolerite dykes and sills. The Permo–Triassic period was later followed by Upper Jurassic–Lower Cretaceous period, which

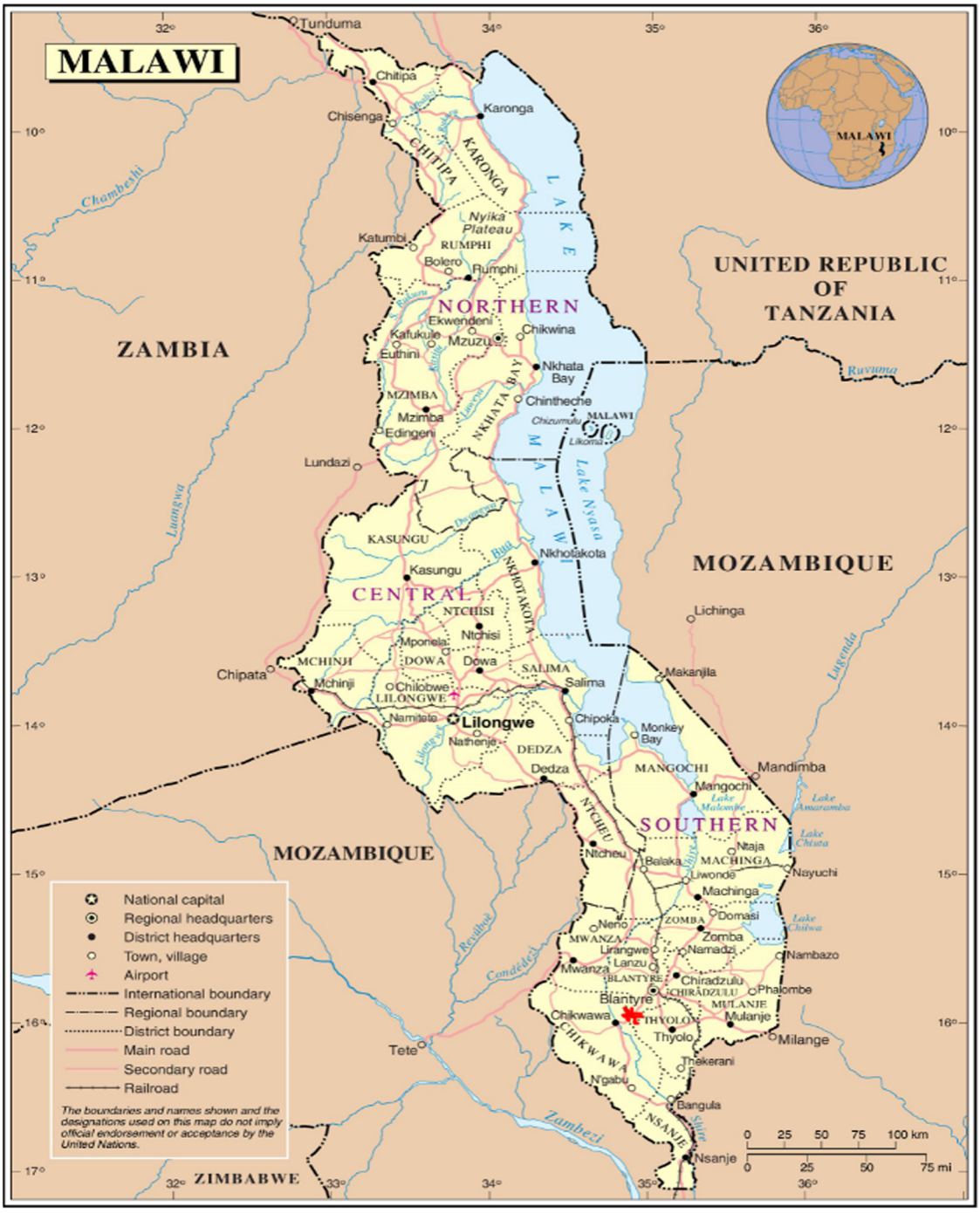

Figure 3: Location of study site on a Malawi map (shown by a red star).

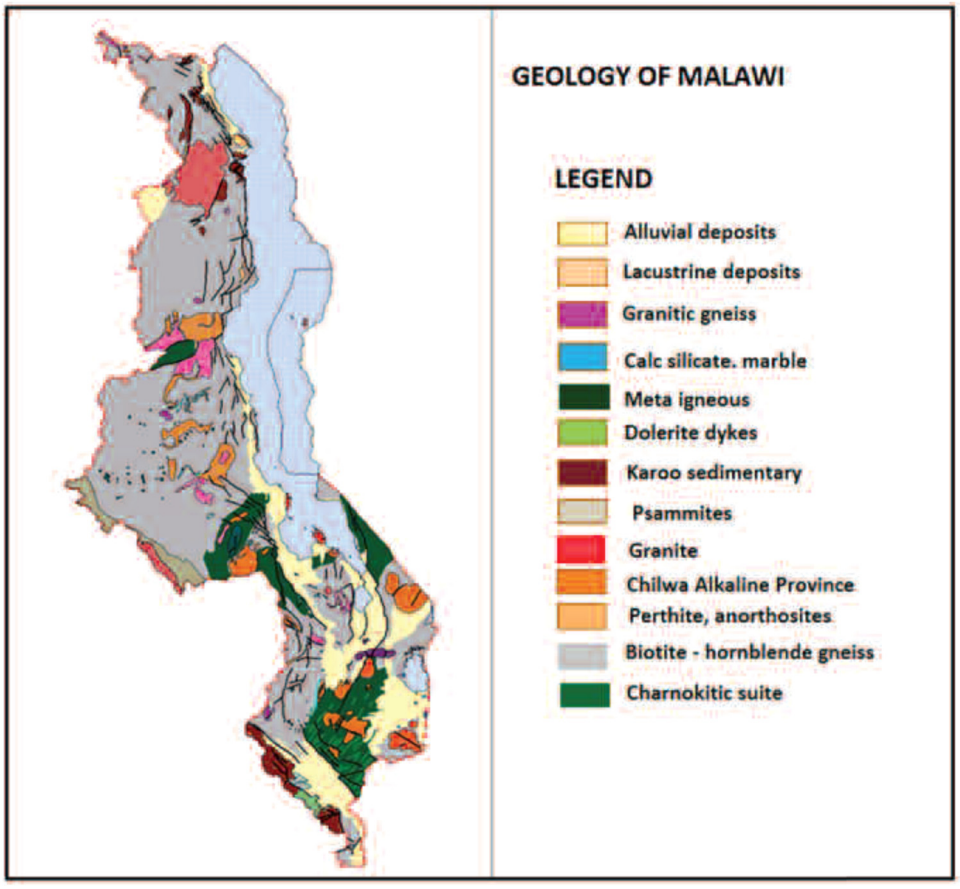

Figure 4: Geology of Malawi [27].

saw the intrusion of syeno-granitic and nepheline syenite rocks later intruded by volcanic rocks infilled by carbonatite and alkaline dykes. As shown in Figure 4, the Southern part of Malawi is dominated by these rocks and has been grouped as Chilwa Alkaline Province. The same period saw sedimentary deposition characterized by Dinosaur Beds. The aforementioned rocks have been overlain by Tertiary–Pleistocene rocks characterized by consolidated to semiconsolidated beds grouped into Timbiri, Chiwondo, Chitimwe and Alluvial. Minor volcanic activities have been witnessed through the existence of Songwe Volcanics [27]. The study area was chosen because it experiences frequent slope failures and rock falls, which affect economic activities between Blantyre and Chikwawa. In addition, due to its unique geomorphological landscape locally known as Kamuzu View, the area is a popular picnic and entertainment centre.

In order to characterize the rock mass, handmapping was used first, followed by smartphone and finally photogrammetry. The various tools that allowed input data collection are outlined.

2.1 Photogrammetry

Photogrammetric technique required the use of a Nikon D100/Nikon SLR digital camera to take photographs and Agisoft Photoscan/Visual SfM software to create a 3D image point cloud. Photoscan is a photogrammetric program, which matches points between photographs to recreate a mesh in 3D. The software uses Structure from Motion (SfM) and dense multi-view 3D reconstruction algorithms to generate 3D point clouds of an object from a collection of arbitrary taken still images [15]. As most conventional photogrammetric techniques require the coordinates and orientation of the cameras or ground control points (GCPs) to be known to facilitate scene triangulation and reconstruction, the SfM method solves the camera position and scene geometry simultaneously and automatically, using a highly redundant bundle adjustment based on matching features from a set of multiple overlapping images [19,20]. Figure 5 shows an SfM workflow, and Figure 6 shows the delineated 3D image of the study area.

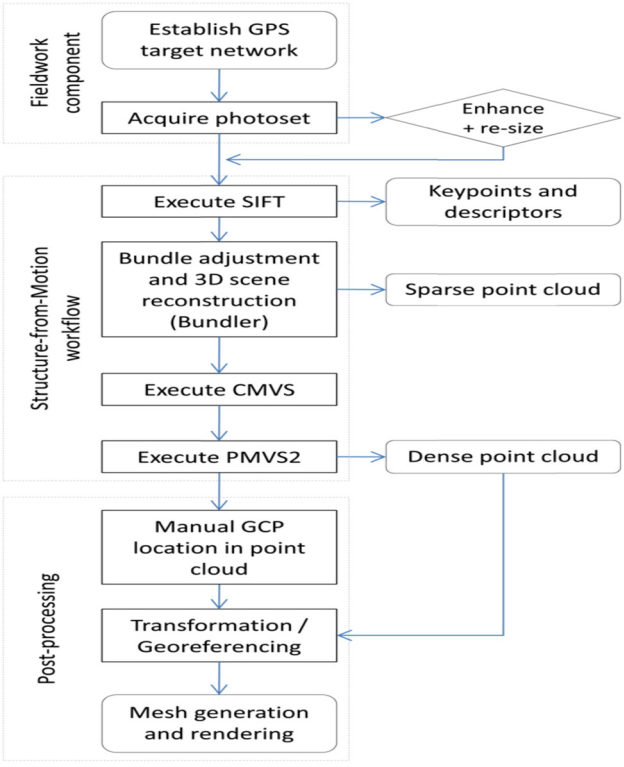

Figure 5: From photograph to point cloud: SfM workflow [20].

2.1.1 3D image and point cloud creation

First, 12 digital images of the rock face were captured from a distance of about 5–10 m using a Nikon camera. In the field, particular attention was taken to maximize overlap by using short camera baselines to obtain well-exposed photographs and uniform coverage of the discontinuities.

The 3D reconstruction pipeline used in Agisoft Photoscan estimates camera calibration parameters automatically utilizing Brown's model for lens distortion removing the need for manual calibration if standard optical lenses and highly redundant image networks are used. For scale and georeferencing, GCPs were added through manual selection, i.e. by adding orientation of a feature on the rock face in each image within the photo set. The alignment process iteratively refines the external and internal camera orientations and camera locations through a least squares solution and builds a sparse 3D point cloud model. Photoscan analyses the source images by detecting stable points and generating descriptors based on the surrounding points [19].

2.1.2 SplitFx processing

The photogrammetric 3D image and point cloud are imported into SplitFx software for manual delineation

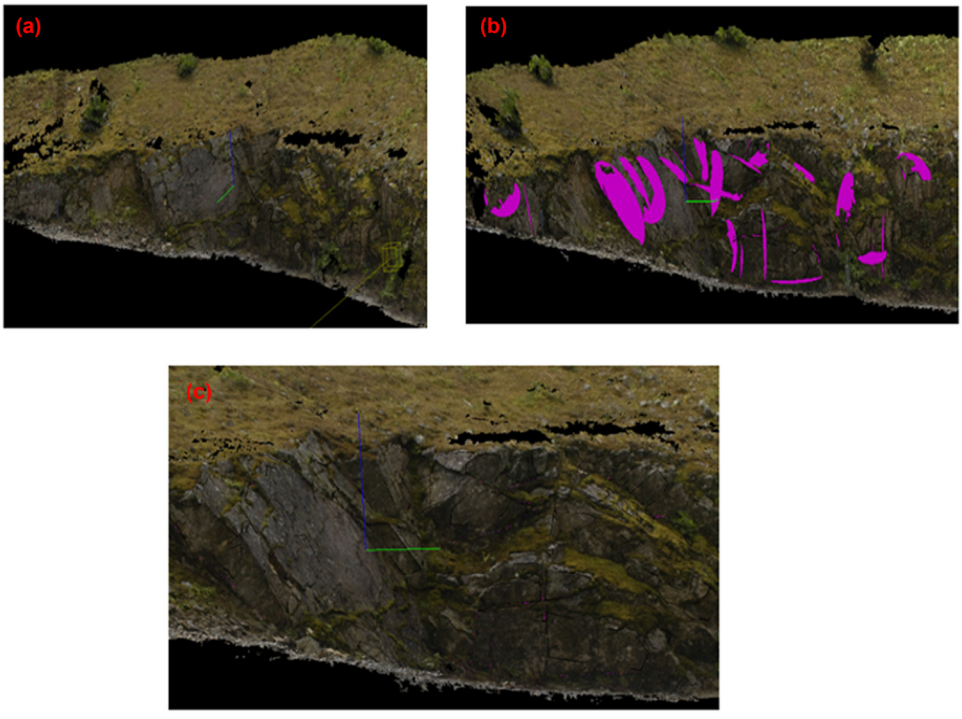

Figure 6: Point cloud 3D image (a) created by photoscan; and delineated in SplitFx showing traces in purple (b); and patches in black (c).

of discontinuities by inserting either planes or traces (Figure 6). The computer mouse is used to select a polygon shape of discontinuities on the point cloud and the SplitFx program identifies the triangle points within the plane to calculate the dip and dip direction of the best fit plane running through the points. Plane recognition is described as a patch in SplitFx software [21]. Similarly, discontinuity traces were identified by manually selecting points along the line of the linear feature and then SplitFx uses the 3D spatial of the selected points to calculate the dip and dip direction. According to ref. [2], orientations of features taken from discontinuity traces are not as accurate as measurements taken from discontinuities represented as planes; therefore, orientations from discontinuity traces were used with care and patch recognition was mostly used to capture orientation data.

2.2 Smartphone (Samsung Galaxy S7)

Through the review of available websites and articles that have considered the use of portable geotechnics [22], several applications that are possible to use in direct or indirect way for geotechnical investigations were applied in geotechnical mapping to compare effectiveness in practice to traditional use of clar compass clinometer and photogrammetry at a road cut. In addition, rockmass classification (RMR and *Q*) was done using the android application *in situ*. This research used Samsung Galaxy S7 for application testing and reviewing.

2.2.1 Data capture

The phone's accelerometer, gyroscope and magnetometer were utilized to collect discontinuity orientation data and create reports *in situ*. Accelerometer detects the orientation of the phone, while the gyroscope tracks the rotation or twist from the information supplied by the accelerometer. The magnetometer provides orientation in relation to the Earth's magnetic field. First, the phone's magnetometer and orientation sensor had to be calibrated by setting both the clar compass and smartphone compass to a reference plane, typically true north, i.e. laying them on a level surface until they gave a similar orientation reading. Additionally, the smartphone's calibration was done by waving the phone in a Figure 8 pattern [23]. Two different geological compass applications (Rock Logger and Geostation) installed on the Samsung Galaxy S7 smartphone were tested.

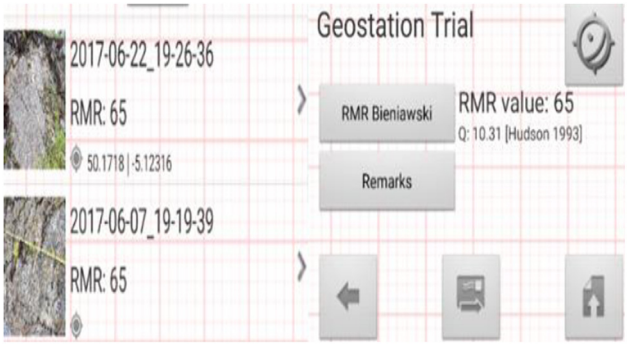

Figure 7: Geostation screenshot.

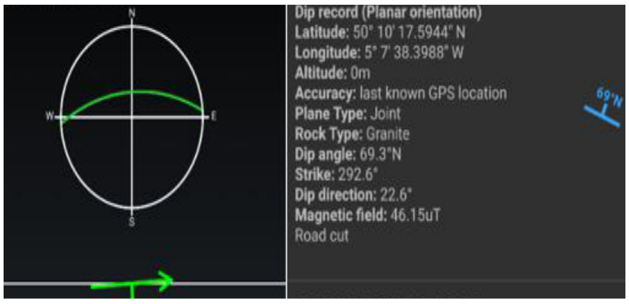

Figure 8: Rocklogger screenshot.

2.2.1.1 Geostation

This geomechanical station application measures the dip, dip direction and strike of discontinuity sets using the smartphone as a compass clinometer. In addition, geomechanical classification by the RMR and the *Q*-system is indicated (Figure 7). The project list was empty at the start of the project, so first, a project was created using the Add New button. Then, dip/dip direction was measured, using the smartphone's compass clinometer high fidelity sensors by placing the smartphone on the joint plane and then pressing Add Disc relocating the device for each structure along the discontinuity.

2.2.1.2 Rocklogger

Rocklogger is a geological/geotechnical tool for measuring the orientation of rock outcrops and plotting a stereonet. It uses the phone's compass and orientation sensors to measure dip and dip direction, or dip and strike, in a single click. GPS and magnetic field information is also saved, along with details on the rock plane and type (Figure 8). After measuring the dip/dip direction

with a clar compass clinometer, the same scanline was mapped using rocklogger to measure the dip/dip direction. Care was taken to map similar discontinuities to the clar compass to obtain a better platform for comparison of orientation data. The app took advantage of the smartphone's compass and orientation sensors higher update speed to measure the dip/dip direction. The smartphone calculates the steepest angle for the dip and uses the direction to calculate the new dip direction.

Normal (planar) orientation mode was used instead of axial orientation mode to log and define plane types. In the planar mode, angle readings are similar whether the phone is oriented screen down or screen up. This allowed underside of rocks to be measured. Azimuth mode was used instead of Quadrant mode to ensure the consistency of orientation data and further use in Dips Rocscience software.

2.2.1.3 Geocam Ar

Geocam Ar is a powerful camera and reporting tool designed to create and preview photos supplied with geospatial information such as geographic coordinates, camera orientation and comments. This app was used to get georeferenced images and view direction (azimuth) of the mapped section, thereby keeping accurate track of mapped faces. The app took advantage of the Galaxy S7 powerful rear camera (12 megapixel) to capture road cut slope details (Figure 9).

2.3 Handmapping

Initially, the granite rock mass was handmapped using a clar compass clinometer to get the dip/dip direction. A clean planar rock face (Figure 10) was selected that is large relative to the size and spacing of the discontinuities exposed. Intersections between discontinuities and the rock face produced linear traces, which provided an essentially 2D sample of the discontinuity network. The 25 m long scanline comprised of a measuring tape pinned to the rock face (often irregular) along its strike and line of maximum dip. The location, orientation and condition of the discontinuities along the scanline were recorded in a booking sheet. Digital photographs were also used together with hand mapping to capture common features for easy identification.

3 Results

3.1 Stereographic analysis

3.1.1 Handmapping (clar compass)

During the geotechnical site investigation, 111 discontinuity measurements were made along the 25 m scanline, which took 6 h to finish. The discontinuity data were analysed using DIPS 7.0 software. The results are summarized in Table 1 and Figure 11.

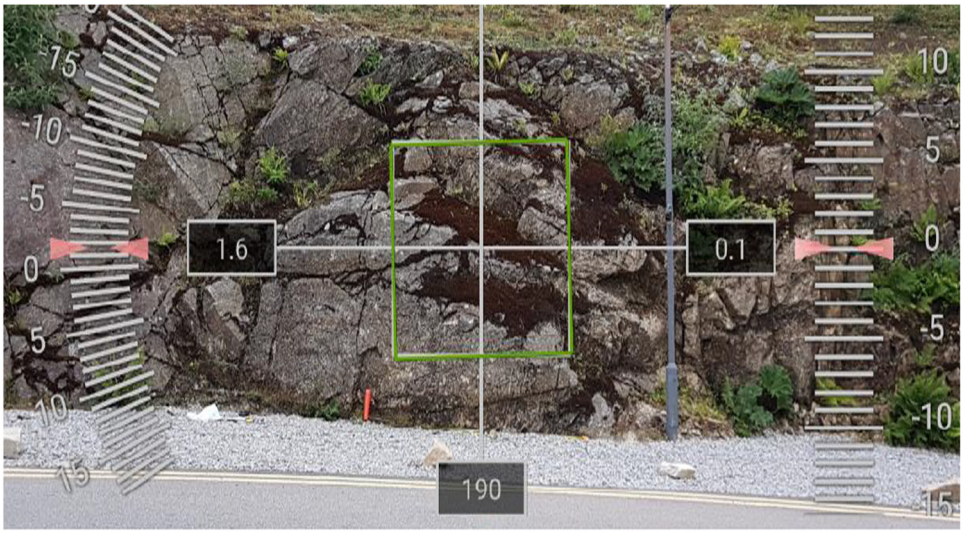

Figure 9: Georeferenced image of road cut looking South West.

Figure 10: Scanline set up on the road cut face. Hammer for scale (33 cm).

Table 1: Summary of joint set characteristics

Set	Type	Dip (°)	Dip direction (°)	No. of poles	Fisher *K*	Average spacing (m)	Description
1	Joint	80	321	28	50.702	0.31	Rough and irregular undulating joints with moderately weathered surfaces
2	Joint	87	198	34	39.392	0.34	As 1
3	Joint	75	266	15	25.5619	0.43	As 1, but occurring only randomly
4	Joint	40	021	23	14.7797	0.27	As 1, but occurring only randomly

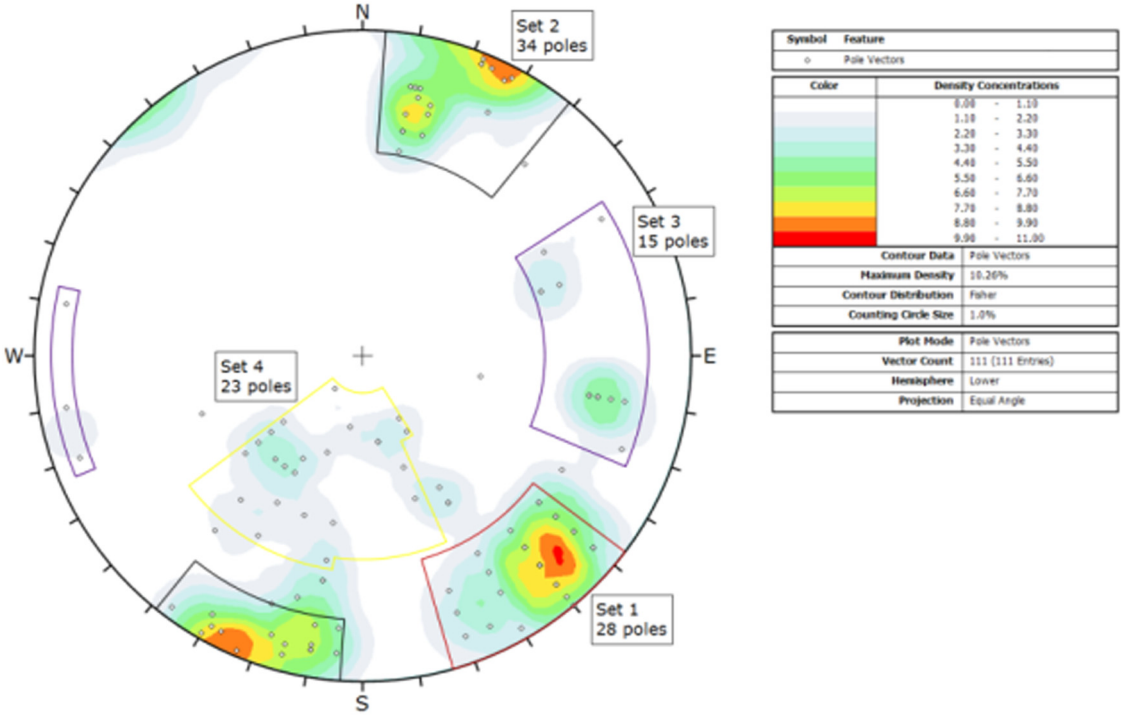

Figure 11: Lower hemisphere stereonet showing set analysis on hand mapped data.

Table 2: Summary of joint set characteristics

Set	Type	Dip (°)	Dip direction (°)	No. of poles	Fisher *K*
1	Joint	73	329	36	69.5
2	Joint	90	207	35	39.2
3	Joint	61	268	9	35.4
4	Joint	47	026	13	22.2

Sets 1 and 2 are the main sets, while sets 3 and 4 are random. Joint sets 1 and 2 are characterized by steeply inclined planes with joint spacing ranging between 200 and 600 mm, while joint sets 3 and 4 are characterized by sub-vertical and sub-horizontal orientation, respectively.

Sets 1 and 2 represent a tighter cluster due to larger Fisher *K* values of 51 and 39, respectively, while sets 3 and 4 have a more dispersed cluster due to smaller Fisher *K* values of 26 and 15, respectively.

The Fisher *K* value describes the tightness or dispersion of an orientation cluster [24]. These *K* values have been estimated using probabilistic analysis for Fisher statistical distribution in Dips RocScience software.

3.1.2 Photogrammetry

Dips software was used to visualize the feature orientation identified in SplitFx. Table 2 shows the dip/dip direction and Fisher *K* of joint sets, and Figure 12 shows a stereonet of the joint sets for easy visualization of density concentration.

3.1.3 Smartphone

During the geotechnical site investigation, 111 discontinuity measurements were made along the 25 m scanline, which took 2 h to finish. The discontinuity data were analysed using DIPS 7.0 software. The results are summarized in Table 3 for Geostation and Table 4 for Rocklogger.

3.1.3.1 Geostation

The orientation data collected using this application were input into dips software to get joint sets (Figure 13) and set statistics (Table 3) for comparison with the other mapping techniques. Set window intervals were done in similar manner to the data from other techniques.

Sets 1 and 2 represent a tighter cluster due to a larger Fisher *K* value of 62 and 40, respectively. Sets 3 and 4 have a more dispersed cluster due to smaller Fisher *K* values of 34 and 17, respectively.

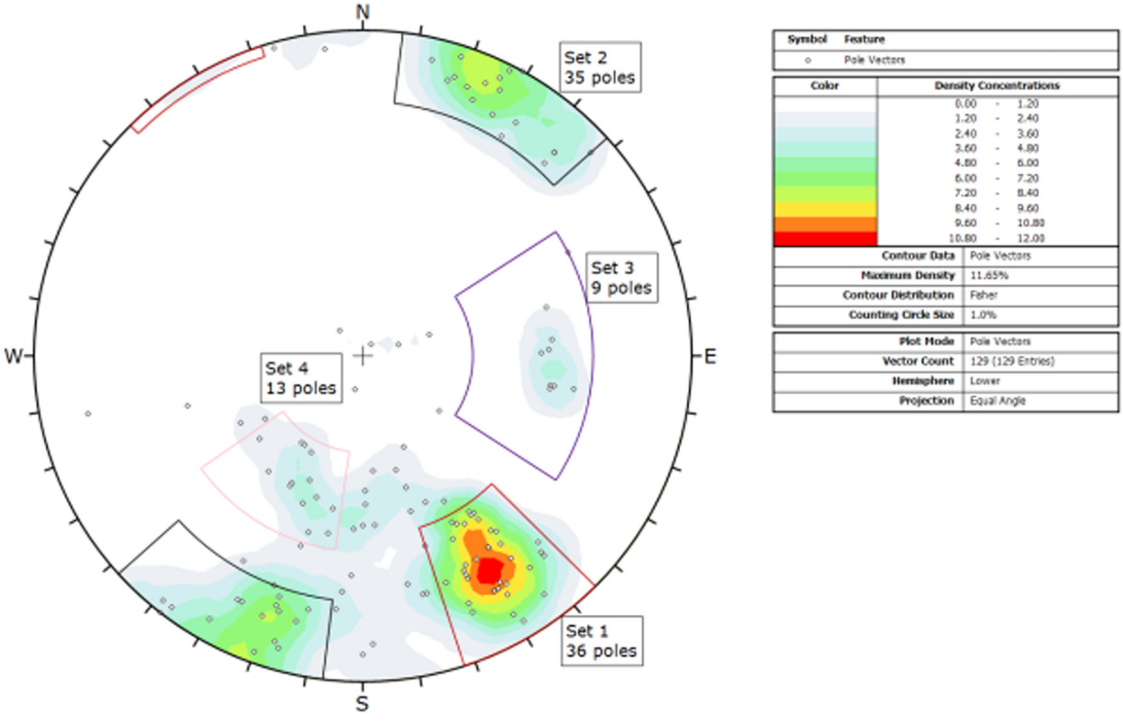

Figure 12: Lower hemisphere stereonet showing set analysis on photogrammetric captured data.

Table 3: Summary of joint set characteristics

Set	Type	Dip (°)	Dip direction (°)	No. of poles	Fisher *K*
1	Joint	82	323	30	62.274
2	Joint	86	195	28	39.5258
3	Joint	73	269	18	34.423
4	Joint	49	027	11	17.195

Table 4: Summary of joint set characteristics

Set	Type	Dip (°)	Dip direction (°)	No. of poles	Fisher *K*
1	Joint	81	322	29	60.5444
2	Joint	89	202	39	38.9822
3	Joint	71	264	11	32.2718
4	Joint	48	027	15	20.59

3.1.3.2 Rocklogger

Similarly, the orientation data collected using rocklogger were input into dips software to get joint sets and set statistics.

Set 1 represents a tighter cluster due to a larger Fisher *K* value of 61, while set 4 has a more dispersed cluster due to a smaller Fisher *K* value of 21.

3.1.3.3 RMR and *Q* value

The Geostation app also calculates the RMR and *Q* value based on the input values. The obtained RMR (65) classifies the rock as a good rock (Table 5). This closely agrees with the RMR76 and GSI rating of 60 based on *Q′* in Table 13. The *Q* value (10.3) from the app slightly varies but the rating puts the rock in the fair to good rock category, which is reasonably similar. Hence, the app can be used right in the field and for quick preliminary rock mass analysis saving the trouble of using the RMR and *Q* tables.

3.2 Set analysis (handmapping, photogrammetry and smartphone)

Orientation data collected from handmapping are compared to the photogrammetric and smartphone data as shown in Tables 6–9. The dip and dip direction recorded by handmapping were used as the reference orientation of each identified plane, so that any differences derived by the other methods were measured as errors or variations in orientation. Four comparable joint sets were identified.

Table 5: Rock mass classification of road cut

(a) Classification parameters and ratings		
Parameter	**Values**	**Rating**
Strength		
Uniaxial compressive strength	50–100 MPa	7
Point load strength index	2–4 MPa	
Drill core Quality RQD	50–75%	13
Discontinuities		
Spacing of discontinuities	200–600 mm	10
Discontinuity length (persistence)	1–3 m	4
Separation (aperture)	0.1–1.0 mm	4
Roughness	Slightly rough	3
Infilling (gouge)	None	6
Weathering	Moderately weathered	3
Groundwater		15
Inflow per 10 m tunnel length	None	
Joint water pressure (major principal stress)	0	

(b) Adjustment for discontinuity orientations		
Applied to:	Slopes	
Strike and dip orientations	Very favourable	0
Obtained RMR value	65	

(c) Rockmass classes determined	
Class number	II
Description	Good rock
Average stand-up time (tunnel face)	1 year for 10 m span
Cohesion of rockmass	300–400 kPa
Friction angle of rockmass	35–45°
Modulus of deformation Em	30 GPa

3.2.1 Comparison of mean set planes

Table 6 shows that joint sets 1 and 2 are characterized by steeply inclined planes, while joint sets 3 and 4 are characterized by sub-vertical and sub-horizontal orientation, respectively.

Table 6 shows less variance in measured dip/dip directions among the three methods. For dip, the standard deviations vary from 4.9 to 9.5°, while their mean values vary from –2 to 2.75°. For dip directions, the standard deviations vary from 3.2 to 4.3°, while their mean values vary from –6 to 0.75°. An acceptable tolerance

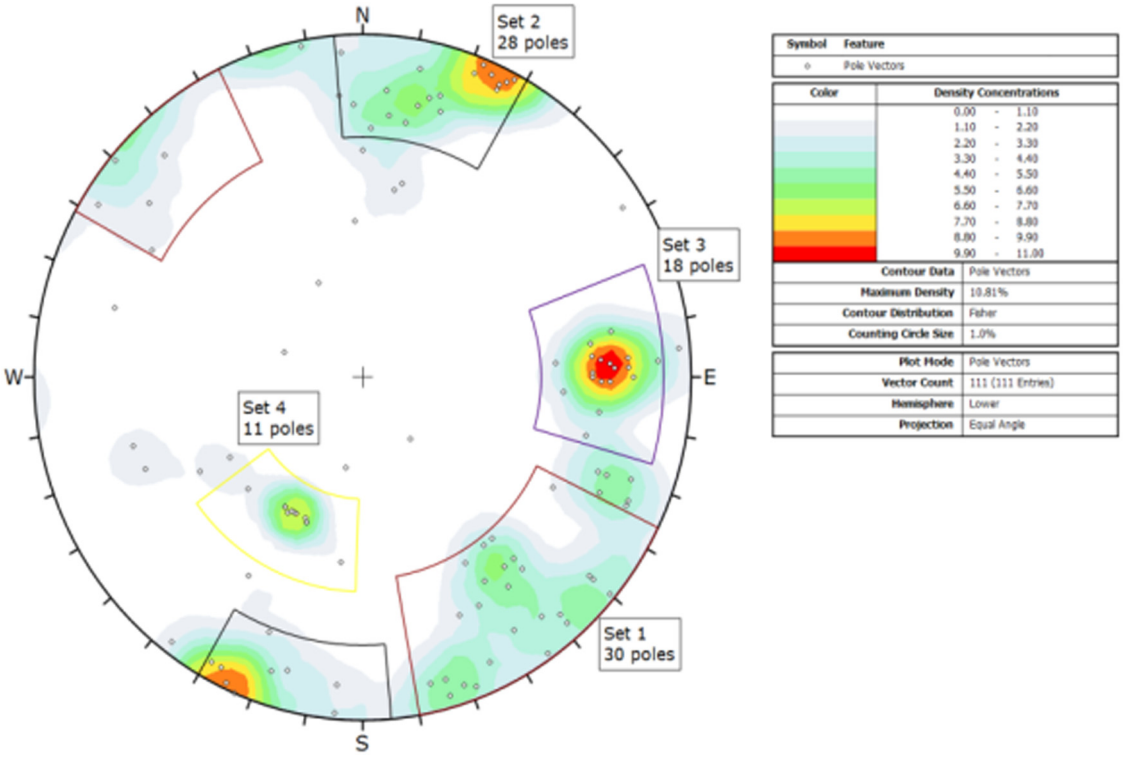

Figure 13: Lower hemisphere stereonet showing set analysis on smartphone captured data using Geostation.

Table 6: Dip/dip direction of joints measured with a clar compass and various smartphone applications (diff – difference between clar and application in red ink)

Set	Handmapping (Clar) (Dip/dip dir)	Photogrammetry (diff)		Geostation (diff)		Rocklogger (diff)	
1	80/321	73/329	7/−8	82/323	−2/−2	81/322	−1/−1
2	87/198	90/207	−3/−9	86/195	1/4	89/202	−2/−4
3	75/266	61/268	14/−2	73/269	2/−3	71/264	4/2
4	40/021	47/026	−7/−5	49/027	−9/−6	48/027	−8/6
Standard deviation			9.5/3.2		5/4.2		4.9/4.3
Mean			2.75/−6		−2/−1.75		−1.75/0.75

Table 7: Fisher *K* coefficient

Set	Handmapping Fisher *K*	Photogrammetry Fisher *K*	Smartphone (geostation) Fisher *K*	Smartphone (rocklogger) Fisher *K*
1	50.7022 (28)[a]	69.5 (36)	62.274 (30)	60.5444 (29)
2	39.392 (34)	39.2 (35)	39.5258 (28)	38.9822 (39)
3	25.5619 (15)	35.4 (9)	34.423 (18)	32.2718 (11)
4	14.7797 (23)	22.2 (13)	17.195 (11)	20.59 (15)
Average	**33.61**	**41.58**	**38.35**	**38.10**

[a] Values in bracket indicate number of poles

limit or error between handmapping and remote data capture systems should be below ±15° [2,26]. For this research, the field orientation measurements between the three different mapping methods of the discontinuities are acceptable since they fit within this allowable error. According to ref. [25], these errors are expected to

Table 8: PVD of field orientation measurements

Set	Handmapping Dip/DipDir (°)	Photogrammetry Dip/DipDir (°)	PVD from handmapping	Smartphone (geostation) Dip/DipDir (°)	PVD from handmapping	Smartphone (rocklogger) Dip/DipDir (°)	PVD from handmapping
1	80/321	73/329	10.46	82/323	2.81	81/322	1.40
2	87/198	90/207	9.48	86/195	3.16	89/202	4.47
3	75/266	61/268	14.12	73/269	3.51	71/264	4.43
4	40/021	47/026	7.80	49/027	9.93	48/027	9.01
		Average	**10.47**	**Average**	**4.85**	**Average**	**4.83**

Table 9: Summary of failure modes by slope face dip and varying dip direction due to bending nature of the road cut

Direction of sliding	South West	North East	East	South East	South East
Dip/dip direction	75/021	75/198	75/266	75/321	75/330
Planar (with limits)	Yes Set 4 (47.8%)	No	No	No	No
Wedge	Yes Sets 1 and 4 Sets 3 and 4	No	No	Yes Sets 3 and 4	Yes Sets 1 and 4 Sets 3 and 4
Toppling (flexural)	No	No	No	No	No

be around 5° for dip angle and around 10° for dip direction. Photogrammetry shows slightly higher variation in dip but lower variation in dip direction as compared to smartphone. This is likely to be due to the low point density or spatial resolution of the 3D triangular mesh.

3.2.2 Comparison of Fisher *K* coefficient

Dips Rocscience software was used to calculate the Fisher *K* values for each joint set. A tight data cluster around the mean orientation was for the steeply dipping sets, one and two, as they had higher average Fisher *K* values. The E–W striking set had lower *K* values than the NE–SW striking set for each mapping technique. The lowest Fisher *K* values resulted from the shallowest dipping set, set 4. The average Fisher *K* values across each set for each mapping tool are shown in Table 7.

3.2.3 Comparison of pole vector difference (PVD)

Based on comparable orientation sets identified by handmapping, smartphone and photogrammetry, their PVDs are illustrated in Table 8. Sets 1, 2, 3 and 4 are observed in all mapping tools. Overall, handmapping vs photogrammetry gave the highest average PVD of 10.47, while handmapping vs smartphone gave the lowest PVD of 4.8°. Both smartphone applications, Geostation and Rocklogger, can be used for geotechnical mapping as they gave a lower PVD variation of 0.02 (4.85–4.83). The data in this research comprised of 100 patches and 29 traces.

3.3 Kinematic analysis

Kinematic analysis has been undertaken using DIPS 7.0 software to identify likely failure modes on the road cut. A friction angle of 35° is used based on Table 5 for rock mass classification and due to the observation that all the surfaces are rough. The lower limit of 35° is assumed to account for the possible effects of groundwater. The results of the kinematic analysis are summarized in Table 9.

Table 10: Summary of planar sliding kinematic analysis results

Planar sliding	Critical	%	Total
All vectors	14	12.61	111
Set 4: J4	11	47.83	23

Table 11: Summary of wedge sliding results

Intersection type	Critical 1	%	Critical 2	%	Total
Grid data plane intersections	1,082	17.79	748	12.30	6,083
All set planes	574	15.71	402	11.00	3,653
Set 1 vs set 2 planes	46	4.83	86	9.03	952
Set 1 vs set 3 planes	58	13.81	25	5.95	420
Set 1 vs set 4 planes	158	24.53	205	31.83	644
Set 2 vs set 3 planes	166	32.55	0	0.00	510
Set 2 vs set 4 planes	24	3.07	50	6.39	782
Set 3 vs set 4 planes	122	35.36	136	39.42	345
User and mean set (unweighted) plane intersections	1	10.00	2	20.0	10
User plane intersections	No results				
Mean set plane (unweighted) intersections	0	0.00	2	33.33	6

Based on direct observation of the slope in the field, it was decided to report the highest relevant percentage of joints (or intersections) for the Dips analysis of each failure mode where this is 20% or more of the total and 30% or more of one set, otherwise "*N*" not to be considered further. The slope face has a dip of 75° and a dip direction of 330° which varies due to the bending nature of the rock face. Failure can only occur where the dip of the single plane or line of intersection of a wedge is shallower than the apparent dip of the slope in the direction of potential sliding and steeper than the effective angle of frictional resistance. The criteria in which the dip direction of the plane must be within ±20° dip of slope only apply to planar failure. Based on this primary test, only set 1 might control planar failure (Table 10) as it does satisfy the failure condition. In addition, wedge failure is likely due to sets 1, 3 and 4 whose dip is less than the slope face dip. Set 2 presents a low risk as it does not satisfy both failure criteria.

The percentage of critical intersections compared to the total number is high (set 4: 48%) and poses a risk so planar sliding is a concern for this slope orientation and friction angle.

For set 3 and 4 intersection type, the percentage of critical intersections (critical 1: 35% and critical 2: 39%) compared to the total number (345) poses a risk, so wedge sliding is a concern for this slope orientation and friction angle (Table 11). Also, sets 1 and 4 have potential to cause wedge failure as the percentage of critical intersections is slightly high compared to all poles. This shows that set 4 has a dominating influence on stability. Only sets 3 and 4 daylight hence will be used in *Q*-slope stability analysis.

As shown in Table 12, flexural toppling is not a great concern for the slope as the percentage of critical intersection is zero.

3.4 Rock mass classification

GSI values have been obtained by direct reading of the GSI charts, conversion from RMR (RMR76′) and *Q*′. The results of the GSI determination are summarized in Table 13. RQD obtained from mapping of exposures typically ranges from 50 to 75%. The mean RQD for determination of GSI is taken as 63%. Ratings for joint spacing and condition used to generate a rock mass classification are based on the most critical discontinuities (sets 3 and 4) of the road cut.

For obtaining a *Q*′ value, it was considered that there are four joint sets, leading to a joint set number Jn of 15. An alternate Jn of 12 representing three joint sets plus random produces *Q*′ values which are not significantly different from those produced for four joint sets.

3.4.1 *Q*-slope

The following *Q*-slope ratings were assigned to the road cut for wedge and planar failure analysis (Table 14).

3.4.1.1 Wedge failure analysis

Sets 3 and 4 control wedge failure. Based on the assigned ratings, *Q*-slope and β were estimated as follows:

Table 12: Summary of flexural toppling results

Flexural toppling	Critical	%	Total
All vectors	0	0.00	111

Table 13: Summary of rock mass classification

Parameter	Rating	Comments
Q'	6.3	***Q'*** (= RQD/J_n × J_r/J_a) RQD = 63; joint set number, J_n = 15; joint roughness number, J_r = 1.5; joint alteration number, J_a = 1
9logeQ' + 44	61	GSI from Q'
GSI direct	60	Blocky/fair to good – perhaps 55 to 65 ≥ 60
RMR76′	60	Uniaxial compressive strength, UCS = 50 MPa ≥ 7; RQD = 63 ≥ 13; spacing: 0.3–1 m ≥ 20; condition ≥ 20
Average GSI	**60**	

Table 14: *Q*-slope ratings

Parameter	Rating	Comments
RQD	50–75% = 63%	Fair to good rock
J_n	15	Four or more joint sets, random, heavily jointed
J_r	1.5	Rough and irregular undulating joints with moderately weathered surfaces
J_a (set 4)	1	Unaltered joint walls, surface staining only
J_a (set 3)	0.75	Tightly healed
O-factor (set 4)	0.75	Orientation adjustment for joints in rock slope. Set 4 is dominant and unfavourable
O-factor (set 3)	1	Set 3 is less dominant and quite favourable. But it will be considered due to potentially unstable wedge formation
Jwice	0.6	Wet environment, competent rock but unstable structure
SRFa – physical condition**	5	Loose blocks and susceptibility to weathering
SRFb – stress**	1	Moderate stress–strength range (σ_c/σ_1: 50–200)
SRFc – major** discontinuity	2	Unfavourable

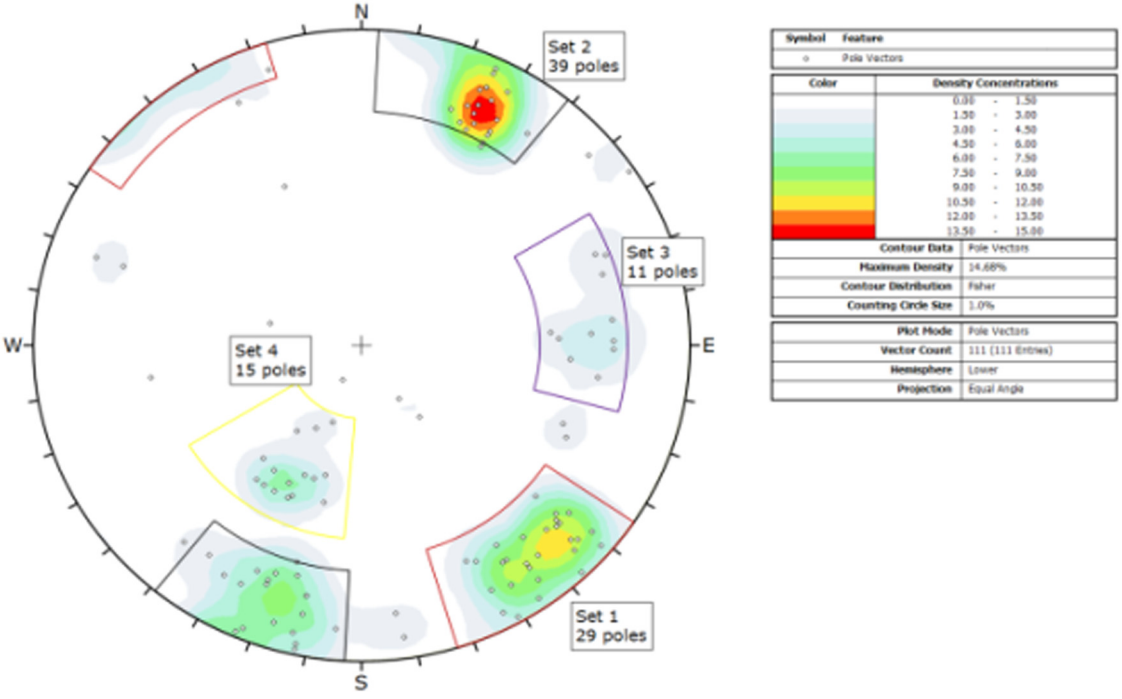

Figure 14: Lower hemisphere stereonet showing set analysis on smartphone captured data using Rocklogger.

$$Q\text{-slope} = 63/15 \times [(1.5/1 \times 0.75) \times (1.5/0.75 \times 1)] \times 0.6/5 = 1.134. \quad (1)$$

Therefore, the steepest slope angle (β) not requiring reinforcement or support to prevent wedge failure is as follows:

$$\beta = 20 \log 10(1.134) + 65° = 66°. \quad (2)$$

In Figure 13, the blue cross shows that the existing slope angle (75°) is unstable but the suggested Q-slope angle of 66° (the red cross) will increase the stability of the road cut (Figures 14 and 15).

3.4.1.2 Planar failure analysis

Set 4 controls planar failure. Based on the assigned ratings, Q-slope and β were estimated as follows:

$$Q\text{-slope} = 63/15 \times [(1.5/1 \times 0.75)] \times 0.6/2.5 = 0.567. \quad (3)$$

Thus, the steepest slope angle (β) not requiring reinforcement or support to prevent planar failure is as follows:

$$\beta = 20 \log 10(0.567) + 65° = 60°. \quad (4)$$

Similarly, Figure 16 shows that the existing slope angle of 75° is unstable (blue cross) and hence the suggested Q-slope angle of 60° needs to be used to increase slope stability (red cross).

4 Discussion and conclusion

Comparative application of photogrammetry, handmapping and android smartphone for geotechnical mapping and slope stability analysis raises questions concerning the appropriate accuracy, reliability and scale of mapping needed to effectively characterize a rock mass. The author successfully applied photogrammetry, android smartphone and handmapping to collect and compare discontinuity orientation data at a road cut along Blantyre–Chikwawa, Malawi. The rock mass orientation data were further used for kinematic analysis to identify potential modes of slope failure. Access to slope face for conventional mapping was limited due to safety concerns. The results of this research showed that android-smartphone

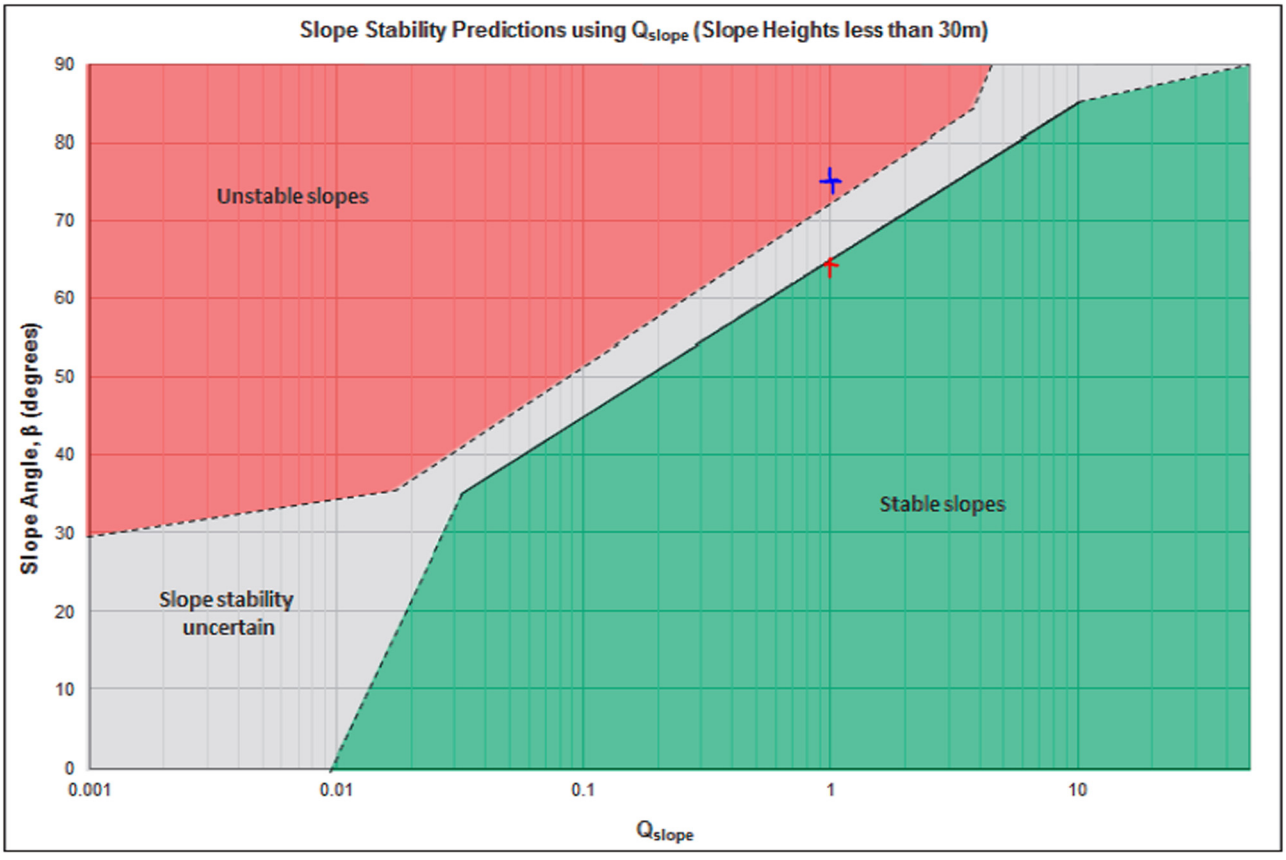

Figure 15: Q-slope stability chart for road cut.

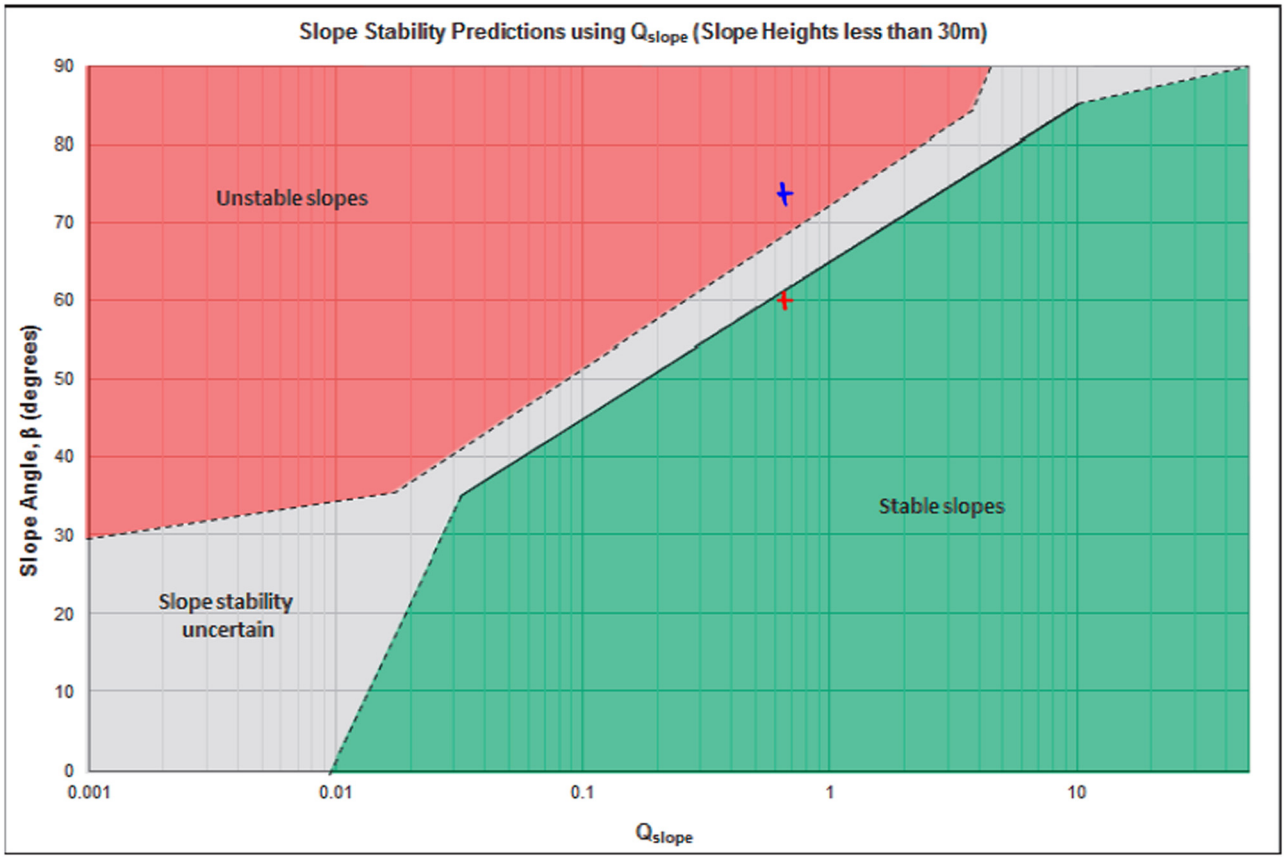

Figure 16: *Q*-slope stability chart for road cut.

has a role in geotechnical mapping since the pole vector error and standard deviation given by smartphone orientation data as compared to handmapped data are less than ±15°. Set analysis on 111 comparable data points gave a maximum PVD of 10.5°, with the minimum having a difference of 4.8°. For dip, the standard deviations vary from 4.9 to 9.5°, while their mean values vary from −2 to 2.75°. For dip directions, the standard deviations vary from 3.2 to 4.3°, while their mean values vary from −6 to 0.75°. In the present study, the field orientation measurements between the three different mapping methods of the discontinuities provided a reasonably acceptable representation of the orientation of the fracture network on the rock mass and they fit within the allowable orientation error of ±15° although photogrammetry showed slightly higher variation in dip but lower variation in the dip direction as compared to smartphone. This is likely to be due to the low point density and spatial resolution of the 3D triangular mesh. According to ref. [25], these errors are expected to be around 5° for dip angle and around 10° for the dip direction. Overall, handmapping vs photogrammetry gave the highest average PVD of 10.47°, while handmapping vs smartphone gave the lowest PVD of 4.8°. Both smartphone applications, Geostation and Rocklogger, can be used for geotechnical mapping as they gave a lower PVD variation of 0.02 (4.85–4.83). A tight data cluster around the mean orientation was observed for the steeply dipping joint sets, 1 and 2, as they had higher average Fisher *K* values. The E–W striking joint set had lower Fisher *K* values than the NE–SW striking joint set for each mapping technique applied. The lowest Fisher *K* values resulted from the shallowest dipping joint set 4. Stereographic and kinematic analysis showed that the 75° dipping road cut is predominantly prone to wedge failure with minor planar failure since the percentage of critical intersections for joint sets 3 and 4 is high compared to all poles. For slope stability, *Q*-slope suggested a new slope angle within the range of 60–66°. The major drawback with smartphone usage is safety, as the user still needs physical contact with the rock face to collect discontinuity orientation data. In addition, magnetic fields locally affect smartphones hence the need to check with clar compass for calibration and georeferencing purposes, i.e. level and align with respect to the magnetic and true North.

The research findings of this study will assist mining companies, road authorities and civil and building

contractors in carrying out geotechnical assessments for various engineering projects using a smartphone due to its portability, less survey time and lower cost as compared to a clar compass, Nikon Camera, Total Station and LIDAR. Technology is still at its infancy in Malawi such that there is a need to create University engineering programs that will stimulate the students to be innovative and creative. Therefore, the research output from the present study will also promote the use of smartphones in geotechnical engineering undergraduate programs and foster research as well as policy that has an impact on the safety of the society.

In order to address the smartphone site safety concern, it is recommended that future work should investigate the 3D image quality of reconstructed rock slopes using different android and iOS smartphones for remote data collection, delineation and slope monitoring as probably the type of smartphone camera used might influence the results obtained. Discontinuity orientation, persistence and intensity are the main inputs required for the generation of discrete fracture network models [15]. The time is fast approaching that a new ISRM Suggested Method for Remote Rock Mass Data Capture should be developed [2].

Acknowledgments: The author would like to thank University of Malawi, The Polytechnic for supporting this research.

Conflict of interest: The author has not declared any conflicts of interest.

References

[1] Priest SD. Determination of discontinuity size distributions from scanline data. Rock Mech Rock Eng. 2004;37(5):247–386.

[2] Coggan JS, Wetherelt A, Gwynn XP, Flynn ZN. Comparison of hand-mapping with remote data capture systems for effective rock mass characterization. In: Sousa LR, Olalla C, Grossmann NF, eds., 11th congress of the international society for rock mechanics. Lisbon, Portugal: Taylor & Francis; 2007. p. 201–6.

[3] Piteau DR. Engineering geology contribution to the study of stability of slopes in rock with particular reference to De Beers Mine. Ph.D. Thesis. University of the Witwatersrand, Johannesburg, South Africa; 1970

[4] Sztubecki J, Bujarkiewicz A, Derejczyk K, Przytuła M. Displacement and deformation study of engineering structures with the use of modern laser technologies. Open Geosci. 2020;12:354–62. doi: 10.1515/geo-2020-0051.

[5] Knapen BV, Slob S. Identification and characterisation of rock mass discontinuity sets using 3D laser scanning. The Geological Society of London; 2006 (AEG 2006 Paper number 438).

[6] Francioni M, Sciarra N, Ghirotti M, Borgati L, Salvini R, Calamita F. The impact of new technologies in the engineering classification of rock masses. Italian J Eng Geol Environ. 2019;2019:33–9. doi: 10.4408/IJEGE.2019-01.S-06.

[7] Ozturk HS, Kocaman S, Gokceoglu C. A low-cost approach for determination of discontinuity orientation using smartphone images and application to a part of Ihlara valley (central Turkey). Eng Geol. 2019;254:63–75. doi: 10.1016/j.enggeo.2019.04.011.

[8] Can R, Kocaman S, Gokceoglu C. A convolutional neural network architecture for auto-detection of landslide photographs to assess citizen science and volunteered geographic information data quality. ISPRS Int J Geo-Inf. 2019;8(7):300. doi: 10.3390/ijgi8070300.

[9] Kocaman S, Gokceoglu C. A CitSci app for landslide data collection. Landslides. 2019;16(3):611–5. doi: 10.1007/s10346-018-1101-2.

[10] World Bank. Mineral sector review: Source of economic growth and development, report no. 50160-MW. Washington D.C: The World Bank; 2009.

[11] Slama I. Manual of photogrammetry. 4th edn. Virginia, US: American Society of Photogrammetry; 1980.

[12] Wolf PR, Dewitt BA. Elements of photogrammetry, with applications in GIS. 3rd edn. Boston: McGraw-Hill; 2000.

[13] Krosley LK, Shaffner PT, Oerter E, Ortiz T. Digital ground-based photogrammetry for measuring discontinuity orientations in steep rock exposures. Proceedings: 41st US symposium on rock mechanics, Golden, Colorado, 17–21 June; 2006.

[14] Martin CD, Tannant DD, Lan H. Comparison of terrestrial-based, high resolution, LiDAR and digital photogrammetry surveys of a rock slope. In: Eberhardt E, Stead D, Morrison T, eds., Proceedings of the 1st Canada-U.S. Rock mechanics symposium, vancouver, 27–31 May; 2007. p. 37–44.

[15] Sturzenegger M, Stead D. Close-range terrestrial digital photogrammetry and terrestrial laser scanning for discontinuity characterization on rock cuts. Eng Geol. 2009a;106:163–82. doi: 10.1016/j.enggeo.2009.03.004.

[16] Bieniawski ZT. Engineering rock mass classifications: A complete manual for engineers and geologists in mining. Civil and Petroleum Engineering. New York, NY: Wiley; 1989.

[17] Hoek E. Strengths of rock and rock masses. Int Soc Rock Mech NJ. 1994;2(2):4–16.

[18] Barton NR, Bar N. Introducing the *Q*-slope method and its intended use within civil and mining engineering projects. In: Schubert W, ed., Future development of rock mechanics; proc. ISRM reg. symp. eurock & 64th geomechanics colloquium, Salzburg 7–10 October; 2015. OGG; p. 157–62.

[19] Thoeni K, Giacomini A, Murtagi RK, Kniest E. A comparison of multi-view 3D reconstruction of a rock wall using several cameras and a laser scanner. The international archives of the photogrammetry, remote sensing and spatial information sciences, vol XL-5, ISPRS technical commission V symposium, 23–25 June 2014, Riva del Garda, Italy; 2014.

[20] Westoby MJ, Brasington J, Glasser NF, Hambrey MJ, Reynolds JM. Structure-from-motion. Geomorphology. 2012;179:300–14. doi: 10.1016/j.geomorph.2012.08.021.

[21] Split Engineering. SplitFX user manual, beta version 1. Arizona, US: Split Engineering LLC; 2005.
[22] Djuric U, Dragana P, Marjanovic M, Kuzmic P. Portable geotechnics-using android smartphones and tablets for geotechnical field investigations. Geo Conf Inf Geoinf Remote Sens Bulgaria. 2013;1:513–20. doi: 10.5593/SGEM2013/BB2.V1/S08.
[23] RockGecko. Rocklogger. Accessed on www.rockgecko.com; 2019.
[24] Fisher R. Dispersion on a sphere. Proc R Soc Lond. 1953;A217:295–305.
[25] Windsor CR, Robertson WV. Rock reinforcement practice. Rock mass formulation, vol 1; 1994.
[26] Gwynn XP. Assessment of remote data capture systems for the characterisation of rock fracture networks within slopes. PhD Thesis. Camborne School of Mines, University of Exeter; 2007.
[27] Malunga G. The geology and mineral potential of Malawi. Technical File. Mining and trade review; 2018.